Excited-State Structural Dynamics of Propanil in the S-2 State: Resonance Raman and First-Principle Investigation

ARTICLE *in* THE JOURNAL OF PHYSICAL CHEMISTRY B · JUNE 2012

Impact Factor: 3.3 · DOI: 10.1021/jp3034853 · Source: PubMed

4 AUTHORS, INCLUDING:

Xuming Zheng
Zhejiang Sci-Tech University
109 PUBLICATIONS **1,263** CITATIONS

SEE PROFILE

THE JOURNAL OF PHYSICAL CHEMISTRY B

Article

pubs.acs.org/JPCB

Excited-State Structural Dynamics of Propanil in the S_2 State: Resonance Raman and First-Principle Investigation

Kemei Pei,* Mingyang Su, Lin Chen, and Xuming Zheng

Department of Chemistry and State Key Laboratory of Advanced Textiles Materials and Manufacture Technology and Engineering Research Center for Eco-dyeing and Finishing of Textiles, Ministry of Education, Zhejiang Sci-Tech University, Hangzhou 310018, China

Supporting Information

ABSTRACT: Resonance Raman (RR) spectra and quantum chemical calculations were used to investigate the photodissociation dynamics of propanil in the S_2 state. The RR spectra indicate that the photorelaxation dynamics for the $S_0 \rightarrow S_2$ excited state of propanil is predominantly along nine motions: C═O stretch, ν_{51} (1659 cm^{-1}), ring C═C stretch, ν_{50} (1590 cm^{-1}), NH wag/ring C═C stretch, ν_{49} (1534 cm^{-1}), ring CCH in-plane bend/NH wag, ν_{42} (1383 cm^{-1}), NH wag/$-CH_2-$ rock, ν_{41} (1353 cm^{-1}), ring C═C stretch/NH wag/$-CH_2-$ rock in-plane, ν_{40} (1299 cm^{-1}), Ph−NH stretch/ring CCH in-plane bend, ν_{37} (1236 cm^{-1}), ring CCH in-plane bend, ν_{35} (1150 cm^{-1}), $-CH_2CH_3$ twist, ν_{33} (1080 cm^{-1}), ring trigonal bend, ν_{31} (1029 cm^{-1}), ring CCH bend out-of-plane, ν_{27} (899 cm^{-1}), whole skeleton deformation in-plane, ν_{20}(688 cm^{-1}). Strong electron coupling between S_1 and S_2 of propanil is found by quantum chemistry calculations and depolarization spectra. The excited-state dynamics of the S_2 state is discussed, and the results are compared with the previously reported results for formanilide to examine the Cl substitution effect.

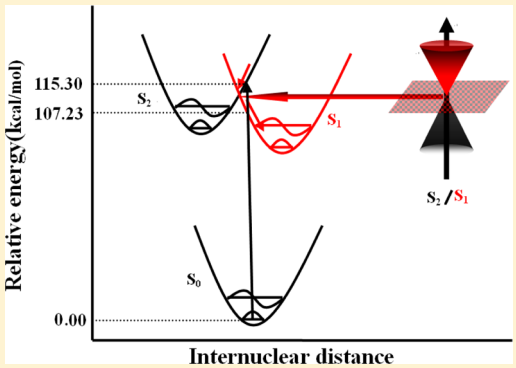

INTRODUCTION

Propanil (3′, 4′-dichloropropionanilide) is a selective contact herbicide used worldwide to control weeds through inhibition of photosynthesis for rice crop production. It is classified as an acylanilide which belongs to the family of phenylamides. Propanil and its major degradation product, 3,4-dichloroaniline (DCA), are biologically active pollutants to the environment. Propanil degradation is directly dependent on the environmental conditions and rate of the pesticide application.[1]As we know, when herbicides are spread in the environment, only a small proportion reaches its target.The excess herbicides are exposed in the sunlight, and photochemical reactions may happen before other chemical processes. Consequently, phototransformation may result from the direct photoexcitation of the excess herbicides by sunlight. Therefore, investigating the photochemical behavior of propanil is very important to pesticide science and environmental science.

Crosby et al. first studied the photodegradation of propanil in an aqueous medium under ultraviolet (UV) and sunlight irradiation, and they found that propanil converts to 3,4-dichloroaniline (3,4-DCA) and other aromatic compounds.[2] The photohydrolysis products depend on the irradiation wavelength. When propanil solution is irradiated at the limit of the absorption band with the lamp emitting mainly at 365 nm, the product of *para*-hydroxylation is the main photoproduct. This wavelength effect is related to the presence of the NH−CO group, since it was also observed with diuron, linuron, and chlorbromuron, and disappears when diuron is methylated on the aromatic nitrogen atom. Furthermore, no wavelength effect was observed with 3,4-dichlorophenol.[3]Tanaka employed ultraviolet lamps and natural sunlight and found that photolysis of monuron, diuron, linuron, metobromuron, and propanil produces halogenated biphenyls according to the photocoupling reaction under investigation. All yields of chlorinated biphenyls from sunlight photolysis were approximately 1% or lower.[4] In recent years interest has been focused on the use of semiconductor materials as photocatalysts for the removal of propanil from the aqueous or gas phase. This method has been suggested in environmental protection due to its ability to oxidize organic and inorganic substrates.[5−9]Transformation of propanil from the direct photoexcitation of the substrate by sunlight or artificial light of shorter wavelengths is an important degradation method in aquatic environments, and previous studies are concentrated on the photoproduct analysis. In contrast with the ultrafast electronic spectra, vibrational spectroscopies such as resonance Raman (RR) spectroscopy and infrared absorption generally reveal detailed information about the molecular and electronic structure as well as photo short-time dynamics in excited states. Few studies have been carried out for propanil in Franck−Condon region short-time dynamic analysis and conical intersection of different potential

Received: April 11, 2012
Revised: June 12, 2012
Published: June 18, 2012

   dx.doi.org/10.1021/jp3034853 | *J. Phys. Chem. B* 2012, 116, 7914−7919

energy surfaces, which often plays an important role in the photodissociation dynamics.

Resonance Raman spectroscopy is a useful tool for probing excited states in the Franck−Condon region because the only modes that contribute appreciable intensity are those most coupled to the electronic excitation. The aim of the present work is to investigate the short-time photodecay dynamics of propanil in a water/menthol solution by resonance Raman spectroscopy and quantum chemistry calculations. Our investigations are expected to be helpful in understanding the photophysical and photochemical characteristics of propanil in the aquatic environment.

EXPERIMENT AND CALCULATIONS

The UV absorption spectrum of propanil was measured by a UV-2501 PC ultraviolet/visible spectrometer. FT-Raman and Fourier transform infrared (FT-IR) spectra of propanil were obtained using a Thermo Nicolet FT-Raman 960 spectrometer and a Perkin-Elmer 1 FT-IR spectrometer, respectively. The methods and experimental apparatus used for the resonance Raman experiments have been described elsewhere.[10−12] Only a short description is given in this paper. The harmonics of a nanosecond Nd:YAG laser and their hydrogen Raman-shifted laser lines were used to generate the 208.8, 245.9, and 252.7 nm excitation wavelengths employed in the resonance Raman experiments. A backscattering geometry was used for sample excitation and for collection of the Raman-scattered light by reflective optics. The Raman-scattered light through a polarizer and entrance slit of a 0.5 m spectrograph and the grating of the spectrograph dispersed the light onto a liquid nitrogen cooled charge-coupled device (CCD) mounted on the exit of the spectrograph. A concentration of approximately 0.005 mol/L in H_2O/CH_3OH (4:1 by volume) solvent is used as the solution-phase sample. The Raman shifts of the resonance Raman spectra were calibrated using the known vibrational frequencies of the solvent Raman bands. The solvent Raman bands were subtracted from the resonance Raman spectra using an appropriately scaled solvent spectrum.

Density functional theory was used to determine the optimized geometry, vibrational frequencies, electronic transition energies, and electronic transition orbitals for propanil. The vibration wavenumber for the ground state, electronic transition energies, and electronic transition orbitals were calculated at the B3LYP TD/6-311+G (d,p) theoretical level. Complete active space self-consistent field (CASSCF) calculations was performed to search for the optimized geometry structures of the S_0, S_1, and S_2 excited states and the surface crossing seam to acquire the optimized geometry structure of the S_2/S_1 conical point . In the CASSCF theory calculations, the active space includes eight electrons and seven orbitals (referred to as CASSCF(8,7)). All quantum mechanical calculations were carried out with the Gaussian09 program.[13]

RESULTS AND DISCUSSION

Absorption Spectra. Figure 1 presents the absorption spectrum of propanil in a water/methanol (4:1 by volume) mixture with the wavelengths for the resonance Raman experiments indicated above the spectrum. Table 1 lists the B3LYP-TD/6-311+G (d,p)-computed electronic absorption bands, the corresponding electric dipole transition orbitals, and the oscillator strengths for propanil. The most stable structure of propanil is discussed in this paper. Table 1 shows

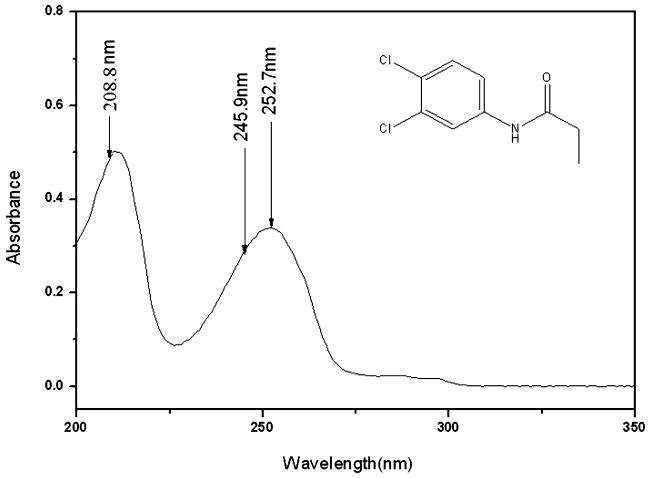

Figure 1. Absorption spectrum of propanil in a water/methanol (4:1 by volume) mixture with the wavelengths for the resonance Raman experiments indicated above the spectrum.

Table 1. B3LYP-TD/6-311+G(d,p)-Calculated Electronic Transition Energies, Oscillator Strengths (f), and Transition Character for Propanil

state	character	orbital	transition energy (eV)	f	exptl
$S_0 \rightarrow S_1$	$^1(\pi, \pi^*)$	55 → 57 (0.31) 56 → 57 (0.10) 56 → 58 (0.61)	4.65 (267 nm)	0.0175	
$S_0 \rightarrow S_2$	$^1(\pi, \pi^*)$	55 → 58 (−0.15) 56 → 57 (0.67)	5.00 (245 nm)	0.4363	251 nm (f = 0.49)
$S_0 \rightarrow S_3$	$^1(n, \pi^*)$	54 → 57 (0.65) 54 → 61 (−0.13) 54 → 62 (−0.13) 54 → 63 (90.11)	5.10 (243 nm)	0.0004	
$S_0 \rightarrow S_4$	$^1(\pi, \pi^*)$	56 → 59 (0.65) 56 → 60 (0.24)	5.15 (240 nm)	0.0004	
$S_0 \rightarrow S_5$	$^1(\pi, \sigma^*)$	56 → 59 (−0.24) 56 → 60(0.64)	5.33 (233 nm)	0.0001	
$S_0 \rightarrow S_6$	$^1(n, \pi^*)$	54 → 58(0.70)	5.74(216 nm)	0.0000	

that among the calculated electronic transitions above the 210 nm optical region there is one transition-allowed absorption band ($S_0 \rightarrow S_2$) at 245 nm with an oscillator strength f = 0.4363. This should be correlated with the intense experimental absorption band at 251 nm with an experimental oscillator strength f = 0.48. Figure 2 displays the four orbitals (55, 56, 57, and 58) associated with the electronic transition of the $S_0 \rightarrow S_2$ transition. It shows that orbitals 55 (HOMO − 1, π) and 58 (LUMO + 1, π^*) are π orbitals with electron density mainly delocalized on the phenyl ring. Orbitals 56 (HOMO, π) and 57 (LUMO, π^*) are orbitals with electron density delocalized on the whole molecule. According to the classic view, we assign

dx.doi.org/10.1021/jp3034853 | J. Phys. Chem. B 2012, 116, 7914−7919

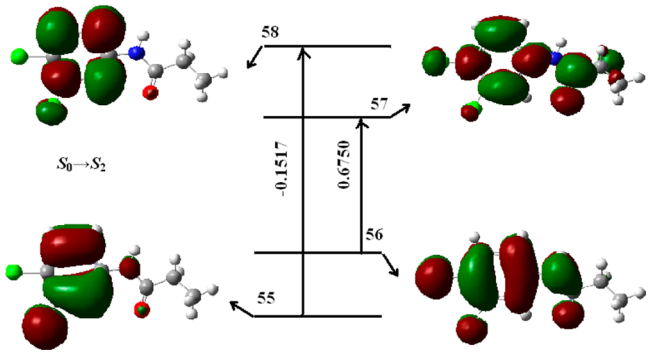

Figure 2. Molecular orbitals for the $S_0 \rightarrow S_2$ transition associated with the 251 nm absorption band of propanil at the B3LYP-TD/6-311+G(d,p) level.

this intense experimental 251 nm absorption band to the π (the whole molecule) $\rightarrow$ π^* (the whole molecule) transition. The 245.9 and 252.7 nm spectra in our resonance Raman experiments are mostly on resonance with the $S_0 \rightarrow S_2$ transition.

Vibrational Analysis and Resonance Raman Spectra. Table 2 lists a comparison of the FT-Raman and FT-IR values. The notations and assignments of the vibrations are based on the visualization GAUSSVIEW 3.0 software. The overall agreement between the linear scaled density functional theory (DFT) calculated vibrational frequencies and the experimental values is good for propanil. The scaled factor for frequencies at the B3LYP/6-311+G (d,p) level is 0.9877.[14] Figure 3 presents an overview and vibrational assignments of the 245.9 and 252.7 nm resonance Raman spectra. The spectra shown in Figure 3 have been corrected for sample reabsorption as well as the wavelength dependence response of the detection system. Solvent Raman bands were removed from the spectra by subtracting an appropriately scaled solvent spectrum.

Figure 3 only indicates the largest Raman band contributions to each Raman feature of the spectra since the intensity of some Raman bands in the spectrum may have contributions from several Raman bands which have very close Raman shifts due to

Table 2. Experimental and B3LYP/6-311+ G(d,p)-Computed Vibrational Frequencies in the Fingerprint Area (500−2000 cm^{-1}) of Propanil (*a*, Scaled by 0.9877)

	computed		experimental			
mode	B3LYP	*a*	R-Raman	FT-Raman	FT-IR	description
ν_{16}	481	475		485s	484w	whole skeleton stretch
ν_{17}	537	530			561w	NH rock out-of-plane
ν_{18}	575	567		588w		whole skeleton deformation out-of-plane
ν_{19}	605	597				whole skeleton deformation out-of-plane
ν_{20}	668	659	688w	688m		whole skeleton deformation in-plane
ν_{21}	704	695				whole skeleton deformation out-of-plane
ν_{22}	706	697				ring deformation out-of-plane
ν_{23}	713	704		725w		whole skeleton deformation in-plane
ν_{24}	811	801				CH_2CH_3 rock/ring CCH out-of-plane
ν_{25}	813	803				CH_2CH_3 rock/ring CCH out-of-plane
ν_{26}	906	894		875w	870m	whole skeleton stretch
ν_{27}	915	903	899w	902w	903m	ring CCH bend out-of-plane
ν_{28}	935	923				$-CH_2CH_3$ rock/NH stretch
ν_{29}	950	938		939m		ring CCH bend out-of-plane
ν_{30}	1021	1008				$-CH_2CH_3$ rock
ν_{31}	1036	1023	1029m	1029s	1029m	ring triangle bend
ν_{32}	1086	1072				$-CH_2CH_3$ rock
ν_{33}	1098	1084	1080w	1076m	1075w	$-CH_2CH_3$ twist
ν_{34}	1139	1124		1128m	1125m	ring CCH in-plane bend/ring breath
ν_{35}	1170	1155	1150w	1153w		ring CCH in-plane bend
ν_{36}	1192	1177			1200s	ring CCH in-plane bend/NH wag/CO−NH stretch
ν_{37}	1245	1229	1236s	1236s	1235m	Ph−NH stretch/ring CCH in-plane bend
ν_{38}	1278	1262		1257w		ring CCH in-plane bend/NH wag
ν_{39}	1289	1273				$-CH_2CH_3$ torsion
ν_{40}	1322	1305	1299m	1298s	1296m	ring C=C stretch/NH wag/$-CH_2-$ rock in-plane
ν_{41}	1375	1358	1353w	1357w		NH wag/$-CH_2-$ rock
ν_{42}	1408	1390	1383w	1384w	1385s	ring CCH in-plane bend/NH wag
ν_{43}	1415	1397				CH_3 umbrella
ν_{44}	1466	1447		1423w		$-CH_2-$ bend symmetry
ν_{45}	1494	1475		1452w		$-CH_3$ deformation
ν_{46}	1500	1481		1463w		ring CCH in-plane bend
ν_{47}	1506	1487		1475w	1474vs	CH_3 scissor
ν_{48}	1533	1514				NH wag/ring CCH in-plane bend
ν_{49}	1614	1594	1534m	1523m	1527vs	NH wag/ring C=C stretch
ν_{50}	1631	1610	1590vs	1591vs	1588vs	ring C=C stretch
ν_{51}	1759	1737	1659m	1664s	1662vs	C=O stretch

dx.doi.org/10.1021/jp3034853 | J. Phys. Chem. B 2012, 116, 7914−7919

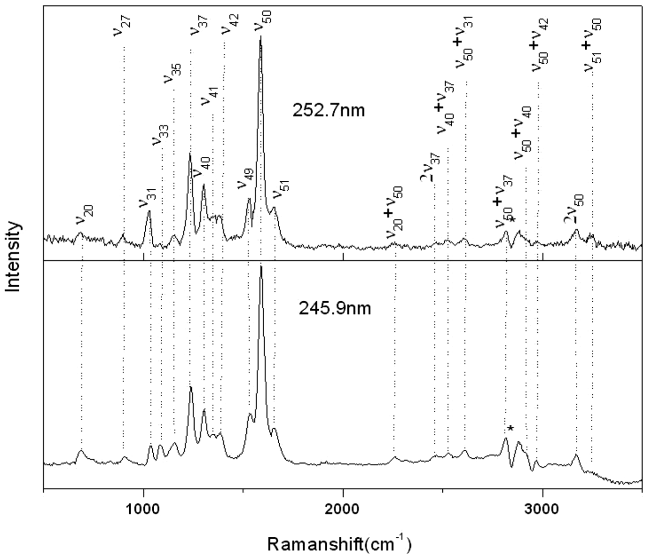

Figure 3. Overview and vibrational assignments of the 245.9 and 252.7 nm resonance Raman spectra of prapanil in a water/methanol (4:1 by volume) solution.

the limited resolution of the solution-phase spectra. Vibrational spectra of formanilide, *N*-(2-methylphenyl)-2,2-dichloroacetamide (2MPA), and *N*-(4-methylphenyl)-2,2-dichloroacetamide (4MPA) were used as references to assign vibrational modes of propanil.[15,16]Most of the resonance Raman features can be assigned to the fundamentals, overtones, and combination bands of Franck−Condon active vibrational modes on the basis of the information presented in Table 2: C═O stretch, ν_{51} (1659 cm^{-1}), ring C═C stretch, ν_{50} (1590 cm^{-1}), NH wag/ring C═C stretch, ν_{49} (1534 cm^{-1}), ring CCH in-plane bend/NH wag, ν_{42} (1383 cm^{-1}), NH wag/$-CH_2-$ rock, ν_{41} (1353 cm^{-1}), ring C═C stretch/NH wag/$-CH_2-$ rock in-plane, ν_{40} (1299 cm^{-1}), Ph−NH stretch/ring CCH in-plane bend, ν_{37} (1236 cm^{-1}), ring CCH in-plane bend, ν_{35} (1150 cm^{-1}), $-CH_2CH_3$ twist, ν_{33} (1080 cm^{-1}), ring trigonal bend, ν_{31} (1029 cm^{-1}), ring CCH bend out-of-plane, ν_{27} (899 cm^{-1}), whole skeleton deformation in-plane, ν_{20} (688 cm^{-1}). Figure 3 clearly shows that the ring C═C stretch vibration, ν_{50}, ring C═C stretch/NH wag/$-CH_2-$ rock in-plane, ν_{40}, and Ph−NH stretch/ring CCH in-plane bend, ν_{37}, dominate the S_2 excited-state structural dynamics of propanil. The result shows the $S_0 \rightarrow S_2$ electron transition weakens the ring C═C bond, strengthens the Ph−NH bond, and rotates the $-CH_2CH_3$ group, and the following S_2 optimized structure at the CASSCF level confirms the RR spectral intensity analysis. It is apparent that in the excited state the energy is not localized in small regions of the conjugated system but spread throughout the molecule for the Franck−Condon region photodissociation dynamics of propanil have multidimensional character, with the motions mainly along 12 vibrational modes, as Figures 2 and 3 show. This energy spread throughout the system phenomenon reflects that propanil has a good energy flow ability. This character leads to large energies of the motions of many atoms within the propanil molecule.

There are some differences between the 245.9 and 252.7 nm RR spectra of propanil, since compared the 245.9 nm RR spectrum the ring trigonal bend, ν_{31}(1029 cm^{-1}), is more intensive and the $-CH_2CH_3$ twist, ν_{33} (1080 cm^{-1}), almost disappears in the 252.7 nm RR spectrum. To check if these differences come from the higher absorption band, the 208.8 nm RR spectrum was obtained and compared with the 245.9 and 252.7 nm RR spectra, as Figure S3 (Supporting Information) shows. It is very clear that there are significant differences between the 208.8 nm RR spectrum and the 245.9 and 252.7 nm RR spectra, for ν_{31} andν_{33} show no activity in the 208.8 nm RR spectrum. That is to say, these small differences of ν_{31} andν_{33} beween the 245.9 and 252.7 nm RR spectra of propanil are not contributed by the 210 nm absorption band. According to Table 1, the oscillator strengths of S_3, S_4, S_5, and S_6 are very small (less than 0.0004), but the oscillator strength of S_1 (0.0145) is relatively large. These facts show the differences beween the 245.9 and 252.7 nm RR spectra of propanil might come from the perturbation from the $S_0 \rightarrow S_1$ excitation.

Comparison to Previous Work on Formanilide. Propanil is a derivative of formanilidel; therefore, comparison between them is performed in this work. Formanilide has a transition-allowed band at 240 nm, which belongs to the π[Ph−NHCOH] → π^*[benzene ring] ($S_0 \rightarrow S_3$) transition.[16] Formanilide is the simplest N-terminal-substituted aromatic amide, and its excited-state charge transfer dynamics was noted to involve the whole molecule after ionization.[17−19] The transition-allowed band $S_0 \rightarrow S_2$ of propanil at 251 nm has been assigned to the π[2Cl−Ph−NHCO] → π^*[2Cl−Ph−$NHCOCH_2CH_3$] transition, as Table 1 and Figure 2 show. Compared with the $S_0 \rightarrow S_3$ transition of formanilide, more delocalization of electron density is found for the $S_0 \rightarrow S_2$ transition of propanil. This greater delocalization character of the electron density means that when propanil absorbs light, the energy can flow easily in the whole molecular structure. That is to say, propanil is stable to irradiation. Compared with the $S_0 \rightarrow S_3$ RR spectra of formanilide, three more active vibrational modes, such as ν_{20} (whole skeleton deformation in-plane, 688 cm^{-1}), ν_{27} (ring CCH bend out-of-plane, (899 cm^{-1}), ν_{33} ($-CH_2CH_3$ twist, 1085 cm^{-1}), ν_{35} (ring CCH in-plane bend, 1150 cm^{-1}), and ν_{41} (NH wag, $-CH_2-$ rock), are found in the RR spectra of propanil. The RR spectra also indicate that propanil has more energy flow ability than formanilide.

Photodissociation Dynamics of Propanil. The electronic state of the 251 nm absorption band of propanil is confirmed to be single or double, since depolarization ratios involve just one resonant electronic state which shows no dispersion (about 1/3). Herein, depolarization ratios for the stronger Raman lines were measured for propanil at 245.9 nm, as shown in the Supporting Information. The depolarization ratios of the C═O stretch, ν_{51}, ring C═C stretch vibration, ν_{50}, NH wag/ring C═C stretch, ν_{49}, ring C═C stretch/NH wag/$-CH_2-$ rock in-plane, ν_{40}, Ph−NH stretch/ring CCH in-plane bend, ν_{37}, and whole skeleton deformation in-plane, ν_{20}, were found to be 0.20, 0.27 0.19, 0.21, 0.50, and 0.81 (all ±0.02), respectively. The values of the depolarization ratios vary with the frequency and exhibit polarization dispersion. The depolarization ratio of ν_{20} in the 245.9 nm RR spectrum deviates from 1/3 significantly .Hence, ν_{20} may contribute to the different components of the electronic transitions for its anomalously polarized Raman line.

The differences between the experimental oscillator strength (0.4363) and calculated oscillator strength (0.49) of $S_0 \rightarrow S_2$ in Table 1 could be explained by the vibronic coupling between adjacent excited states. Further orbital electron density analysis indicates that there is obvious overlap between the S_1 and S_2

dx.doi.org/10.1021/jp3034853 | J. Phys. Chem. B 2012, 116, 7914−7919

states for the S_1 state of propanil has the orbital 56 → 57 contribution, which is the main contribution of $S_0 \rightarrow S_2$. RR spectra of propanil at 245.9 and 252.7 nm are different obviously, since the ring trigonal bend, ν_{31}, is more intensive and teh $-CH_2CH_3$ twist, ν_{33} (1080 cm^{-1}), disappears in teh 252.7 nm RR spectrum, and the above discussion shows that the differences in the 245.9 and 252.7 nm RR spectra come from the $S_0 \rightarrow S_1$ excitation. The S_0, S_1, and S_2 structures are optimized at the CASSCF(8,7)/6-31G(d) level, as Figure S1 (Supporting Information) shows. To check the correctness of the CASSCF method, B3LYP/6-311+G(d,p) structural parameters for the S_0 state are also shown. The optimized standard orientation of the S_0, S_1, and S_2 structures shows that S_0 is in the C_1 point group and S_1 and S_2 are in the C_s point group. Figure S1 clearly shows that the properties of the −NH−CO− bond and −Ph−NH− bond have a small difference. The −NH−CO− bond in the S_1 state is stronger than that in the S_2 state, but −Ph−NH− in the S_2 state is stronger than that in S_1. Figure S1 also shows that the structures between S_1 and S_2 are similar except a little difference for the −NH−CO− bond and −Ph−NH− bond. Table 1 also shows that the vertical transition energies of S_1 and S_2 for propanil are 5.00 and 4.65 eV, respectively, at the B3LYP/6-311+G (d,p) level, only an 8.07 kcal/mol difference. We investigate any possible surface crossing regions near their S_0, S_1, and S_2 stable structures. Since S_1 and S_2 are of C_s symmetry, we start with a structure similar to S_0 but with C_s symmetry at the CASSCF(8,7)/STO-3G level to search the S_2/S_1 conical point, and the above job converged to an optimized conical intersection after six steps. This shows that the starting geometry is near the conical intersection geometry, and the S_2/S_1 point is in teh Franck−Condon region. The S_2/S_1 conical point was confirmed further at teh CASSCF(8,7)/4-31G and CASSCF(8,7)/6-31G(d) levels, and the main bond length and the standard orientation of the S_2/S_1 point at the CASSCF(8,7)/6-31G(d) level are listed in Figure S1 and Talbe S2 (Supporting Information). Because of limited computational resources, we did not check the S_2/S_1 conical point at any higher theoretical level. From the above analysis, we can draw a conclusion that the S_2/S_1 conical intersection may occur in the Franck−Condon region. Figure 4 shows the schematic diagram of the energy relaxation dynamics of propanil in a water/methanol (4:1 by volume) solution.

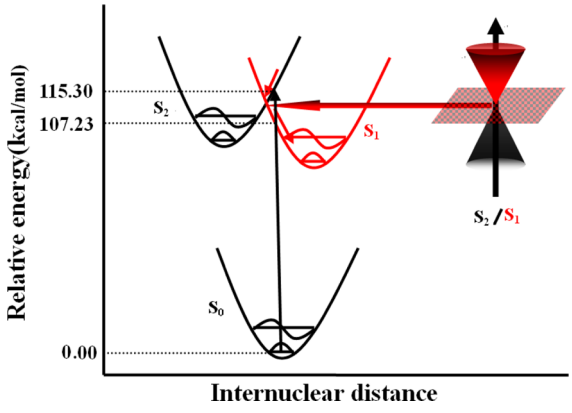

Figure 4. Schematic diagram of the energy relaxation dynamics of propanil in a water/methanol (4:1 by volume) solution.

CONCLUSION

RR spectra of 245.9 and 252.7 nm excitation wavelengths were acquired for propanil in a water/methanol (4:1 by volume) solution. The RR results indicate that the short-time $S_0 \rightarrow S_2$ photorelaxation dynamics of propanil has substantial multidimensional character mainly along the C═O stretch, ν_{51}, ring C═C stretch vibration, ν_{50}, NH wag/ring C═C stretch, ν_{49}, ring CCH in-plane bend/NH wag, ν_{42}, NH wag/$-CH_2-$ rock, ν_{41}, ring C═C stretch/NH wag/$-CH_2-$ rock in-plane, ν_{40}, Ph−NH stretch/ring CCH in-plane bend,ν_{37}, ring CCH in-plane bend, ν_{35}, $-CH_2CH_3$ twist, ν_{33}, ring trigonal bend, ν_{31}, ring CCH bend out-of-plane, ν_{27}, and whole skeleton deformation in-plane, ν_{20}. The RR spectra also indicate that propanil has a stronger energy flow ability than formanilide for strong π bond coupling. Strong electron state coupling was found between the S_2 and S_1 states, and the S_2/S_1 conical intersection can be predicted in teh Franck−Condon region by theoretical and experimental analysis.

ASSOCIATED CONTENT

Supporting Information

RR spectra of the propanil in parallel and perpendicular polarization, depolarization ratios calculated from the 245.9 nm RR spectra, and optimized structures of propanil in the S_0, S_1, and S_2 states at the CASSCF/6-31G(d) level. This material is available free of charge via the Internet at http://pubs.acs.org.

AUTHOR INFORMATION

Corresponding Author

*Phone: +86-571-86843627. Fax: +86-571-86843627. E-mail: peikemei@yahoo.com.cn.

Notes

The authors declare no competing financial interest.

ACKNOWLEDGMENTS

This work was supported by the National Natural Science Foundation of China (Grants 20707023 and 21033002), Natural Science Foundation of Zhejiang (Grant Y5080021), Analysis and Measure Project of Science, Technology Department of Zhejiang Province (Grant 2011C37046), and Zhejiang Top Academic Discipline of Applied Chemistry and Eco-Dyeing & Finishing and Engineering Research Center for Eco-Dyeing & Finishing of Textiles (Zhejiang Sci-Tech University), Ministry of Education of China.

REFERENCES

(1) Darren, R.; Renate, H.; Nick, B.; Andrew, D.; Mohamed, F.; Michael, E.; Peter, E. *BMC Clin. Pharmacol.* **2009**, *9*, 3.
(2) Moilanen, K. W.; Crosby, D. G. *J. Agric. Food Chem.* **1972**, *20*, 950−953.
(3) Amine-Khodja, A.; Boulkamh, A.; Boule, P. *Photochem. Photobiol. Sci.* **2004**, *3*, 145−156.
(4) Tanaka, F. S.; Hoffer, B. L.; Wien, R. G. *Pesict. Sci.* **1985**, *16*, 265−270.
(5) Malato, S.; Blanco, J.; Campos, A.; Caceres, J.; Guillard, C.; Herrmann, J. M.; Fernández-Alba, A. R. *Appl. Catal., B* **2003**, *42*, 349−357.
(6) Malato, S.; Blanco, J.; Caceres, J.; Fernandez, A. R.; Aguera, A.; Rodríguez, A. *Catal. Today* **2002**, *76*, 209−220.
(7) Dhahir, S. A. *Aust. J. Basic Appl. Sci.* **2011**, *5*, 1555−1560.
(8) Fox, M. A.; Dulay, M. T. *Chem. Rev.* **1993**, *93*, 341−357.
(9) Konstantinou, I. K.; Sakkas, V. A.; Albanis, T. A. *Appl. Catal., B* **2001**, *34*, 227−239.

(10) Zhu, X. M.; Zheng, S. Q.; Zheng, X. M.; Phillips, D. L. *J. Phys. Chem. A* **2005**, *109*, 3086−3093.
(11) Wang, H. G.; Liu, B.; Wan, J. M.; Xu, J.; Zheng, X. M. *J. Raman Spectrosc.* **2009**, *40*, 992−997.
(12) Weng, K. F.; Zheng, X. M.; Phillips, D. L. *J. Phys. Chem. A* **2006**, *110*, 851−860.
(13) Frisch, M. J.; Trucks, G. W.; Schlegel, H. B.; Scuseria, G. E.; Robb,M. A.; Cheeseman, J. R.; Montgomery, J. A. J.; Vreven, T.; Kudin, K. N.;Burant, J. C.; et al. *Gaussian 09*; Gaussian, Inc.: Pittsburgh, PA, 2009.
(14) Andersson, M. P.; Uvdal, P. *J. Phys. Chem. A* **2005**, *109*, 2937−2941.
(15) Arjunan, V.; Ravindran, P.; Subhalakshmi, K.; Mohan, S. *Spectrochim. Acta, Part A* **2009**, *74*, 607−616.
(16) Pei, K. M.; Li, F. L.; Zheng, X. M. *J. Raman Spectrosc.* **2011**, *42*, 1034−1038.
(17) Chen, X. B.; Fang, W. H. *J. Am. Chem. Soc.* **2004**, *12*, 8976−8980.
(18) Ullrich, S.; Tarczay, G.; Tong, X.; Dessent, C. E. H.; Muller-Dethlefs, K. *Phys. Chem. Chem. Phys.* **2001**, *3*, 5450−5458.
(19) Ullrich, S.; Tarczay, G.; Tong, X.; Dessent, C. E. H.; Muller-Dethlefs, K. *Angew. Chem., Int. Ed.* **2002**, *41*, 166−168.